 doi:10.20944/preprints202207.0253.v1

Abnormal in LMNA triggers a shift in intracellular metabolic homeostasis via AMPK activation

Ying Zhou[1], Jia-Jie Yang[1], Yuan Cheng[4], Ge-Xuan Feng[1], Rong-Hui Yang[1], Yuan Yuan[3], Li-Yong Wang[2], Lu Kong[1,*]

[1] Department of Biochemistry and Molecular Biology, Capital Medical University, Beijing 100069, China
[2] The central laboratory for Molecular Biology, Capital Medical University, Beijing 100069, PR China
[3] Department of Pathology, Capital Medical University, Beijing 100069, PR China
[4] Department of Physiology, Capital Medical University, Beijing 100069, PR China
* Correspondence: konglu@ccmu.edu.cn; Tel.: (+86-10-83911472-803)

Abstract: Laminopathies are a spectrum of diseases caused by LMNA mutations. In familial partial lipodystrophy of Dunnigan (FPLD), LMNA plays role in the differentiation and development of adipocytes and lipid metabolism. Changes in LMNA predict not only the differentiation of adipose-derived mesenchymal stem cells (AD-MSCs) but also the transformation of cancer cells. Hence, our in-depth study aimed to identify the molecular connection between disordered lipid metabolism and hepatic carcinogenesis. We first discovered significant positive correlations between pLMNA and two key rate-limiting enzymes in *de novo* fatty acid synthesis, acetyl-CoA-carboxylase 1 (ACC1) and fatty acid synthase (FASN), in the liver tissue but not in adipose tissue of obese model rats. Moreover, LMNA knockdown (KD) in rat AD-MSCs prevented the differentiation and maturation of adipocytes. To clarify the mechanistic relationship with lipogenesis, gain- and loss-of-function experiments in which functional changes and the related molecular pathways were investigated in a normal hepatocyte line (7701 cells). Adenosine 5'-monophosphate activated protein kinase α (AMPKα) was found to be activated by abnormalities in the LMNA structure under conditions of LMNA deletion, farnesyltransferase inhibitor (FTI) treatment and LMNA mutations associated with clinical FPLD pathogenic phenotype. Active AMPKα could directly phosphorylate ACC1 and thus inhibit lipid synthesis but induced glycolysis in both HCC cells and normal cells. The HCC cells could not survive with LMNA knockout (KO) or even KD. Lonafarnib (an FTI) combined with low-glucose conditions significantly decreased the proliferation of HepG2 and MHCC cells by inhibiting glycolysis and the maturation of prelamin A.

Keywords: LMNA; AMPK; lipid metabolism; cancer

Preprints (www.preprints.org) | NOT PEER-REVIEWED | Posted: 18 July 2022 doi:10.20944/preprints202207.0253.v1

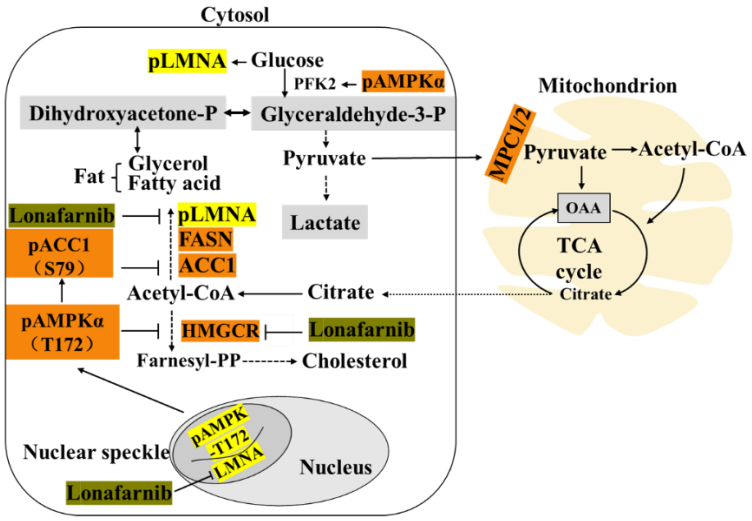

Graphical abstract Adenosine 5'-monophosphate-activated protein kinase α (AMPKα), an energy sensor, coordinates the metabolism of glucose and lipids via its activation of phosphofructokinase 2 (PFK2) in glycolysis and the phosphorylation of its substrate ACC1 in lipogenesis. We first found that abnormal LMNA expression in a normal liver cell line directly recruited activated AMPKα (pAMPKα-T172)and thus changed cellular metabolic homeostasis. Additionally, functions of pLMNA might linked to *de novo* lipid synthesis.

1. Introduction

Lamins on the nuclear envelope belong to the type V intermediate filament family and exist as two types in vertebrates: A and B, which are encoded by *LMNA and LMNB1/B2*, respectively [1, 2]. *LMNA* (also *laminA/C*), located at 1q21.2, contains 12 exons. Prelamin A, the primary RNA transcript, is alternatively spliced into 6 transcript variants: isoform A (Lamin A, 74 kD), isoform C (Lamin C, 65 kD), Isoform ADelta10 (Lamin ADelta10, 71 kD), isoform 4 (64 kD), isoform 5 (63 kD) and isoform 6 (Progerin, 69 kD) [3, 4]. Functional lamin A is generated from prelamin A through four enzymatic processing steps: farnesylation (which guides prelamin A into the nuclear membrane) in a CaaX box (cysteine, 2 aliphatic amino acids, any amino acid), proteolysis of the last three amino acid residues at the carboxy terminus, carboxymethylation, and finally cleavage of the C-terminal 18 amino acids [5-7]. The polymerization of mature lamins A and C and B-type lamins forms the nuclear membrane, assembles the nuclear pore complex and maintains chromatin function, which is involved in many critical molecular events, such as transcription, replication, mitosis, cell cycling, apoptosis, and even cell differentiation [8, 9].

To date, many reports about LMNA-related diseases are available. For example, some evidence supports the function of LMNA as an oncogene in gastrointestinal tract tumors [10], prostate cancer (PC) [11], HCC [12, 13], and metastatic colorectal cancer (CRC) [14-16]. In addition, mutations in *LMNA* induce common laminopathies characterized by multiple rare clinical symptoms, including muscular dystrophy, lipodystrophy, diabetes, dermopathy, neuropathy, leukodystrophy, and progeria [17-19]. Childhood progeria syndrome (Hutchinson-Gilford syndrome, HGPS) is caused by toxic progerin, a truncated variant caused by a point mutation at codon 608 of prelamin A [20]. Several studies have also clarified the underlying mechanism of *LMNA* mutations in progeria-induced ageing and shown the key function of LMNA in promoting the differentiation of myocytes and adipocytes [21-23]. However, the relationship between lipid metabolism and LMNA regulation remains unknown. A case report noted that two biological sisters with *LMNA*-mutant FPLD developed hypopharyngeal squamous cell carcinoma [24].

 doi:10.20944/preprints202207.0253.v1

This study inspired us to focus on the role of LMNA in lipid metabolism associated with metabolic syndrome and HCC [25].

The liver is a central organ well known for its function in coordinating metabolic balance in the human body, and more than 80% of *de novo* fatty acid synthesis occurs in the liver and adipose tissue. HCC development is closely related to metabolic syndrome with fatty liver and insulin resistance. Notably, FPLD is characterized by lipoatrophy of the extremities and, conversely, visceral fat deposition, insulin resistance and hypertriglyceridemia [26]. Aberrant expression of LMNA without mutation has also been reported in human obesity and type 2 diabetes [27, 28]. Thus, metabolic syndrome and HCC should share lipogenesis and factors associated with LMNA regulation. Therefore, we investigated the mechanism by which LMNA modulates triglyceride (TG) synthesis.

Our data suggest that LMNA and its phosphorylated form are involved in different metabolic processes. Mass spectrometry data reveal that LMNA and its partners in the nucleus positively regulate ATP biosynthetic process. AMPK, an ATP or energy sensor, is a "reactor" to abnormal LMNA expression; however, AMPKα activation did not phosphorylate LMNA in our cell models. AMPKα activation was reported to alter *LMNA* splicing and thus reduce progerin production [29].

A pLMNA level was positively correlated with FASN expression during high glucose-induced TG synthesis in 7701, HepG2 and MHCC cells, suggesting the involvement of pLMNA in *de novo* fatty acid synthesis, potentially during mitosis. In addition, LMNA functions as an oncogene in HCC. Therapeutic strategies targeting LMNA mutations or abnormal LMNA expression have recently been validated. Lonafarnib has been approved by the FDA for the treatment of hepatitis D virus (HDV) infection, progeria and progeroid laminopathies. Some experiments have also validated the efficacy of lonafarnib alone for the treatment of HCC [30, 31]. Here, we found that lonafarnib combined with glucose-lowering drugs could effectively inhibit the growth of HCC cells.

2. Materials and Methods

2.1 Cell lines, LMNA-KO cell model and transfection

The 7701 and HepG2 cell lines were obtained from the Department of Cell Biology at Capital Medical University. The MHCC cell line was obtained from the Beijing Institute of Hepatology at YouAn Hospital at Capital Medical University. All cell lines were authenticated. LMNA-KO 7701 cells were generated by CRISPR-Cas9 technology. Six LMNA-sgRNA primer pairs from the Sigma website (listed in Supplementary Table S1) were individually cloned into the pGPU6/GFP/Neo vector (GenePharma, Shanghai, China). Two micrograms of the KO plasmid were transfected into 5×10^5 cells with Lipofectamine 3000 (Life Technologies) for 6 hours, after which the culture medium was exchanged. GFP-positive monoclonal cells were sorted via flow cytometry (FACS Aria II, BD, USA) and cultured in puromycin-DMEM (8119438, Gibco). After one month, stable cells lacking LMNA were acquired. Western blotting verified the LMNA-KO efficiency in the cells, and WT cells were used as a control.

2.2 *Immunohistochemistry (IHC)*

Paraformaldehyde-fixed human liver and adipose tissues (Gift of Professor Wang Miao, Department of Anatomy, Capital Medical University) were subjected to IHC to detect LMNA or pLMNA. The paraffin sections were dehydrated, followed by antigen repair and incubation with hydrogen peroxide. Then, primary antibodies against LMNA (ab133256, Abcam, 1:200) and pLMNA (ab58528, Abcam, 1:2000) were incubated with the sections overnight at 4°C. The next day, the sections were incubated with a secondary antibody (HRP-goat anti-mouse/rabbit IgG polymer, PV-6000, ZSGB-BIO, Shanghai)

Preprints (www.preprints.org) | NOT PEER-REVIEWED | Posted: 18 July 2022 doi:10.20944/preprints202207.0253.v1

for 1 hour. The chromogenic reaction was terminated with DAB substrate (ZLI-9017, ZSGB-BIO, Shanghai). The localization of antibody-positive areas was recorded by fluorescence microscopy (DLMA, Leica), and the sections were photographed.

2.3 RNA extraction and qRT-PCR

Total RNA was extracted with TRIzol (Invitrogen, Carlsbad, CA), FastKing gDNA Dispelling RT SuperMix (KR118-02, TIANGEN, China) and PowerUpTM SYBRTM Green MasterMix (A25742, Applied Biosystems) according to the instructions accompanying the TRIzol. All qRT-PCR primer sequences are listed in a supplemental Table S1.

2.4 Detection of the intracellular TG and lactic acid content

The intracellular TG concentration was measured with a kit according to the instructions (E1013, Applygen, Beijing). First, cells were washed with PBS and then lysed at 25°C for 10 minutes. Then, the protein in 3 μL of lysate was quantified with a BCA protein quantification kit (P0011, Beyotime, Shanghai). The remaining supernatant was transferred to a 1.5-mL centrifuge tube, heated at 70°C for 10 minutes, and then centrifuged at 2000 rpm for 5 minutes at 25°C, after which the supernatant was used for enzymatic assays. A working solution was mixed at a 4:1 ratio (R1:R2) and stored at 4°C. The TG standard was diluted to 6 different concentrations with distilled water to prepare a standard curve, and the control tube contained no TG. All reactions were performed at 37°C for 10 minutes, after which the OD value of each tube was measured.

The TG concentration was calculated based on the protein concentration per mg. A total of 2×10^5 cells in 12-well plates were treated with a conditioned culture medium containing 10% dialyzed serum for 24 hours. Due to the excretion of lactate from the cells into the medium, aliquots of 100 μL of supernatant were collected by centrifugation at 0 and 24 hours. The lactic acid content in the medium was read with an M-100 automatic biosensor/analyzer (Shenzhen Siemen Technology Co., Ltd) and standardized. Standard curves of the excretion or uptake of lactate by the cells per hour were plotted. All data were normalized by comparison with the control.

2.5 Endogenous or exogenous immunoprecipitation assay

A total of 1×10^7 cells were treated with RIPA lysis buffer containing protease inhibitor cocktail (4693116001, Roche, 1:200) and a phosphatase inhibitor (P5641, Sigma, 1:100) on ice for 30 minutes, and the supernatant after centrifugation at maximum speed for 30 min at 4°C was collected. The total protein in a small amount of lysate (input) was assessed using western blot analysis. One to two micrograms of primary antibodies were added to the remaining lysate and incubated for 6 hours at 4°C with slow shaking; these antibodies included anti-LaminA/C rabbit polyclonal antibody (10298-1-AP, Proteintech), anti-phospho-laminA/C (S22) antibody (2026, CST), anti-phospho-laminA/C (S392) antibody (ab58528, Abcam), anti-AMPK alpha 1 antibody(5831, CST), and phospho-AMPK alpha (T172) antibody (2535S, CST). Then, 50 μL of pretreated protein A/G agarose beads (P2055, Beyotime Biotechnology, Shanghai) was added to the cell lysate and incubated overnight with the antibody with slow shaking at 4°C. After the immunoprecipitation reaction, the agarose beads were washed at least 5 times at 4°C. Finally, the beads were resuspended in 2× SDS loading buffer and boiled at 95°C for 10 min. Western blotting was used to analyze protein interactions.

For the exogenous immunoprecipitation assay, plasmids to express the N-terminal region of AMPK (1-312), the C-terminal region of AMPK (331-359) and full-length AMPK were constructed with a vector (pCDHO-puro-3Flag-CMV, GENEWIZ). HEK293T cells (5×106) were transfected with PEI and 10 μg of plasmids. After 48 hours of transfection, the cells were lysed with a cold RIPA reagent for 2 hours. Thirty microliters of the cell

Preprints (www.preprints.org) | NOT PEER-REVIEWED | Posted: 18 July 2022 doi:10.20944/preprints202207.0253.v1

supernatant were collected as the input. The remaining cell lysate was incubated with anti-FLAG beads (A2220, Sigma-Aldrich) at 4°C while rotating overnight. The beads were cleaned three times with a cold RIPA buffer. The final immunoprecipitants were boiled in a 5× SDS loading buffer for immunoblotting.

2.6 Tissue and cell protein extraction, BCA assay and western blot analysis

RIPA lysis buffer and extraction buffer were applied to extract protein from homogenized tissues or cell samples (89900, Thermo Scientific™). A BCA kit (Beyotime, P0011) was used to quantify the protein, and the proteins were then separated by SDS-PAGE. Protein fragments were transferred onto a nitrocellulose (NC) membrane and subjected to immunoblot analysis with the indicated primary antibodies at the following dilutions: anti-laminA/C (10298-1-AP, Proteintech) at 1:1000, anti-phospho-laminA/C (S22) (2026, CST) at 1:1000, anti-phospho-laminA/C (S392) (ab58528, Abcam) at 1:1000, anti-AMPK alpha 1 (5831, CST) at 1:1000, anti-phospho-AMPK alpha (T172) (2535S, CST) at 1:1000, anti-acetyl-CoA carboxylase (21923-1-AP, Proteintech) at 1:1000, anti-phospho-acetyl-CoA carboxylase (S79) (3661S, CST) at 1:1000, anti-FASN rabbit polyclonal antibody (10624-2-AP, Proteintech) at 1:1000, anti-MPC1 (14462, CST) at 1:1000, anti-GAPDH (60004-I-Ig, Proteintech) at 1:5,000, anti-β-actin (60008-1-Ig, Proteintech) at 1:5000, and anti-FLAG (80010-1-RR, Proteintech) at 1:5000 used as a control. The secondary antibodies used were HRP+ goat anti-mouse IgG (H+L) (RS0001, ImmunoWay) diluted at 1:10,000 and anti-mouse IgG (sc-2004, Santa Cruz) diluted at 1:100000. The membranes were developed using an enhanced chemiluminescence HRP substrate (WBKLS0500, Millipore Corporation Billerica, USA) and then exposed to a MiniChemi 610 imager (304002L, SAGECREATION, Beijing, China).

2.7 Extraction and culture of AD-MSCs and their induction

Fresh mouse adipose tissue was digested with 0.075% collagenase (C0130, Sigma) at 37°C for 30 min, filtered into a 100-μm Falcon tube and centrifuged at 1600 rpm for 8 min. The precipitate was resuspended in ammonium chloride for erythrocyte lysis and incubated at room temperature for 5-10 min. An ammonium chloride erythrocyte lysis buffer (storage solution, 10x) containing the following was prepared in a total volume of 1 L: 80.2 g of NH_4CI (15 M), 8.4 g of $NaHCO_3$ (100 mM), and 3.7 g of disodium EDTA (10 mM) in 900 mL distilled water, with the pH adjusted to 7.4. Finally, we added water to bring the volume to 1 L and stored the solution at 4°C for 6 months. The lysate was centrifuged at 3000 rpm for 3 minutes, and the precipitate was washed twice with PBS and 5% serum. The purified AD-MSCs were cultured in six-well plates in F12 medium (SH30023.01, HyClone) containing 10% serum (16000044, Gibco). When the cell density reached 80%-90%, we exchanged the medium for induction differentiation medium A (ready-to-use) at different time points. Induction differentiation medium A (500 mL) contained the following: 0.2 mL of Dex storage solution (1 μM), 0.5 mL of IBMX storage solution (0.5 mM), 0.556 mL of a 4.5 mg/mL insulin solution (5 μg/mL), 0.25 mL of Trog storage solution (5 μM), and 500 mL of DMEM/F-12 complete medium. After 48 hours of cell culture (day 2), the cell morphology changed, and induction differentiation medium A was slowly exchanged with induction differentiation medium B (ready to use); the cells were cultured for an additional 48 hours. Induction differentiation medium B (500 mL) contained the following: 0.556 mL of a 4.5 mg/mL insulin solution (5 μg/mL), 0.25 mL of Trog storage solution (5 μM), and 500 mL of DMEM/F-12 complete medium. After the cells had been cultured for 48 hours (day 4), lipid droplet formation was observed, and the medium was discarded. The medium was exchanged every 2 days until the cells became adipocytes.

2.8 Construction of LMNA phosphorylation mutant plasmids

Preprints (www.preprints.org) | NOT PEER-REVIEWED | Posted: 18 July 2022 doi:10.20944/preprints202207.0253.v1

PCR products containing different mutations were purified, sequenced (Rui Bo Xing Ke Company, Beijing) and then cloned into the pCMV6-AC vector (PS100020, OriGene) to construct plasmids to express the different mutants. Two restriction endonucleases (BamHI and NotI) were used in the cloning process. The plasmids were extracted with the Endotoxin-Free Plasmid Medium Extraction Kit (CW2105s, CW Biotech) and transfected into cells with Lipofectamine 3000 (Invitrogen, 2105082). Western blot analysis was used to verify expression. The mutation primer sequences are listed in Supplemental Table S1.

2.9 High glucose-mediated indication of increased cellular lipid synthesis and oil red O staining

Cells were cultured in standard DMEM (glucose concentration of 5.5 mM) with 10% FBS and 1% streptomycin. After the cells were synchronized by incubation with a serum-free medium for 24 h, they were treated with high-glucose DMEM (glucose concentration of 25 mM). Oil Red O (G1262, Solarbio) staining and TG assays validated intracellular lipogenesis. Specifically, the cells were washed three times with PBS for 5 min and fixed using a 4% paraformaldehyde solution (MFCD00133991, Thermo Scientific™) for 40 min. After the paraformaldehyde was removed, the cells were stained with Oil Red O dye for 30 min at room temperature in the dark. Finally, 60% isopropanol was used for rinsing and decolorization. The treated cells were placed under a microscope for observation and photographed.

2.10 Mass spectrometry

5×10^7 293T cells were lysed and performed nucleoplasmic separation as the manufacturer's suggestions (BioVision, #K266-25). The endogenous immunoprecipitation method was used to precipitate the nuclear protein complexes interacting with LMNA (10298-1-AP, Proteintech). Precipitates were separated via 4%–12% NuPAGE gel (Thermo Scientific, NP0335BOX). Silver-stained was applied using Pierce Silver Stain Kit (Thermo Scientific, 24612). The input was used as a positive control, while IgG was a negative control. Purpose gels were subjected to LC/MS-MS (Agilent 6340) sequencing.

2.11 CCK8 assay

The proliferation of a total of 3000 cells per 96-well plate was assessed after different treatments. A total of 95 μL of medium and 5 μL of CCK-8 reagent (E1CK-000208, EnoGene, Nanjing, Jiangsu Province, China) were mixed and added to the 96-well plate. After incubation for 1-4 hours, the absorbance at 450 nm was determined with a spectrophotometer (Berthold Tristar, 2LB942, Germany).

2.12 Statistical analysis

The western blot, qPCR, co-IP and CCK-8 experiments were repeated at least three times. Prism 8.0 (GraphPad Software, USA) was applied for statistical analysis and plotting. The standard deviation (SD) was calculated. Differences between groups were analyzed by a two-tailed Student's t-test, and the nonparametric test was performed to analyze correlations in the expression of different indexes. $p<0.05$ was used to indicate a statistically significant difference.

3. Results

3.1. Increased pLMNA expression was accompanied by lipogenesis

Obese SD rats were obtained by continuous high-fat diet feeding for 8 weeks. The body weights of some rats fed high-fat food were not significantly higher than those of rats in the control group; these rats were therefore included in the obesity-resistant group. Rats

Preprints (www.preprints.org) | NOT PEER-REVIEWED | Posted: 18 July 2022 doi:10.20944/preprints202207.0253.v1

in the control group were fed the basal diet. Via western blotting, we performed a semiquantitative analysis of changes in FASN, ACC1, LMNA and pLMNA levels in fat and liver tissues from the rats and found pLMNA or FASN levels to be upregulated in the liver tissue of obese rats (highlighted with a red frame), but the difference was not significant, likely due to the limited number of samples (n=5) (Figure 1A). Through correlation analysis, pLMNA levels showed a positive correlation tendency with FASN expression in the obesity model group (Figure 1C). Thus, after the treatment of 7701 and HepG2 cells with high glucose levels (25 mM), lipogenesis was transiently increased (after 12 hours), and oil red O staining was carried out (Figure 1B left). The levels of both FASN and pLMNA were increased, especially in the HepG2 cells, as validated by western blotting (Figure 1B right).

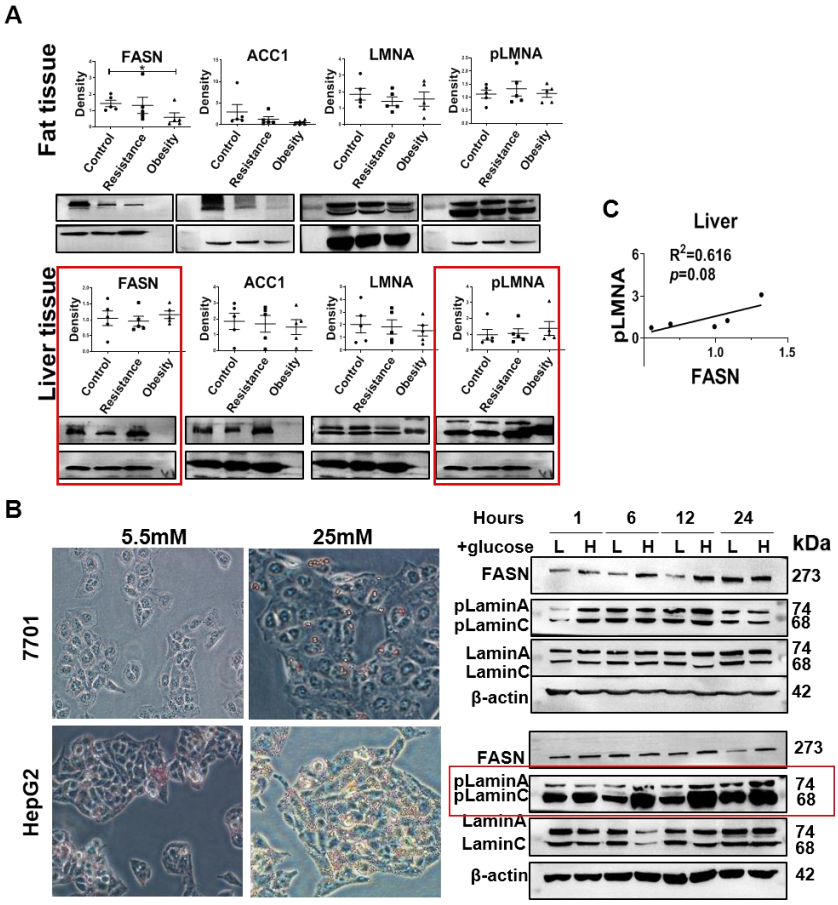

Figure 1. The pLMNA level is elevated in lipogenesis. Obesity was induced in SD rats by continuous high-fat diet feeding for 8 weeks. (A) Representative western blot images showing FASN, ACC1, LMNA or pLMNA levels in adipose and liver tissues from obese rats and the corresponding quantitative graph (n=5). (B) Representative images following Oil red O staining (20×) of 7701 cells and HepG2 cells after treatment with high glucose (25 mM) for 24 hours. Western blotting was used to measure changes in FASN, LMNA and pLMNA levels (n=3). (C) In the obesity model group, pLMNA levels showed a positive correlation with FASN expression. Data are shown as the mean ± SD. ** $p < 0.01$, *** $p < 0.001$. L=5.5mM, H=25mM glucose.

3.2. LMNA KD blocked AD-MSC differentiation and LMNA deletion decreased lipid synthesis in 7701 cells

Lipid biosynthesis occurs in the cytosol, as shown via analysis of LMNA or pLMNA (S392) in human normal liver and fat samples by IHC. We found that pLMNA was

Preprints (www.preprints.org) | NOT PEER-REVIEWED | Posted: 18 July 2022 doi:10.20944/preprints202207.0253.v1

distributed in the area surrounding lipid droplets, suggesting its function in lipid droplet formation (Figure 2A). Furthermore, we isolated AD-MSCs from mice and cultured them. The primary AD-MSCs differentiated into mature adipocytes, which showed strong oil red O staining after eight days by stimulation with a conditional culture medium that contained insulin and dexamethasone (Figure 2B, upper). In addition, we found elevated LMNA levels in the mature adipocytes (Figure 2C, left), and in contrast, the differentiation and proliferation of the AD-MSCs were prevented upon LMNA KD (Figure 2B (down), C (middle) and D). Notably, the deletion of LMNA from the AD-MSCs affected survival (data not shown). The data collected from adipose tissue suggests that LMNA controls the differentiation and proliferation of adipocytes [32]. Fortunately, we obtained 7701 cells in which LMNA had been deleted (Figure 2C, right); these cells showed significantly decreased TG synthesis but increased lactic acid production (Figure 2E) and reduced proliferation (Figure 2D). Interestingly, LMNA was necessary for the survival of HepG2 cells, which share features with AD-MSCs. In summary, LMNA and its phosphorylated form have distinct functions in fat and liver tissues, even during fat synthesis. Clarifying this mechanism will contribute to explaining hyperlipidemia in FPLD.

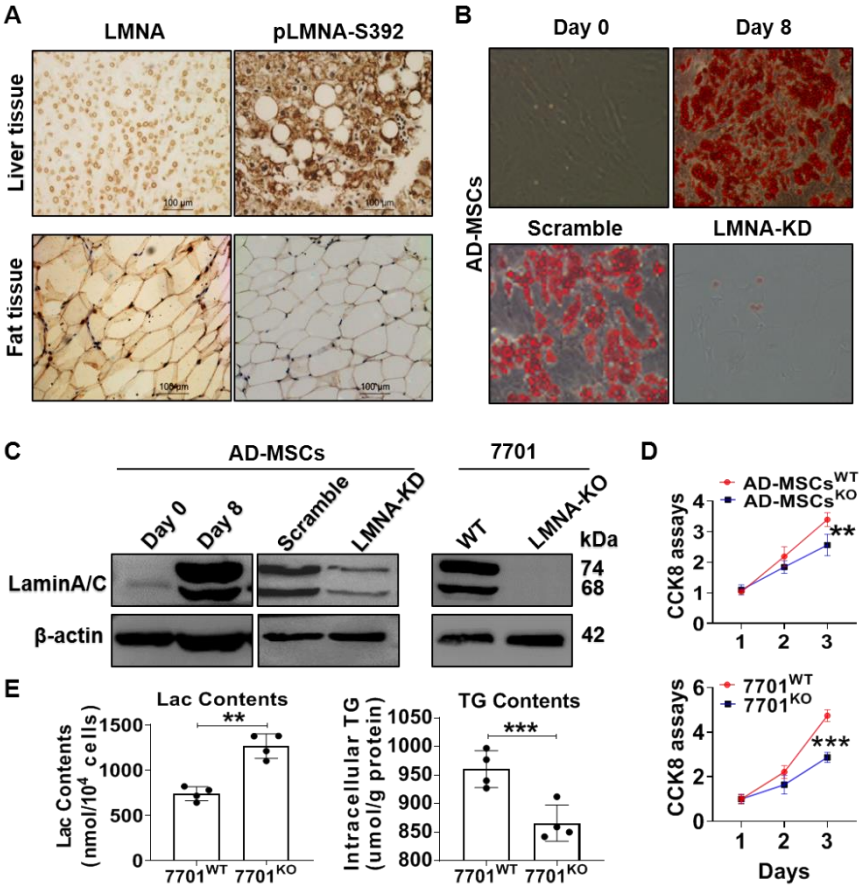

Figure 2. LMNA and its phosphorylation form play different functional roles in metabolism in hepatocytes and adipocytes. (A) Representative IHC images of LMNA and pLMNA-S392 in human adipose and liver tissues (20×). The red circle and arrow indicate pLMNA concentrated around lipid droplets (n=5). (B) Oil red O staining was carried out to show TG synthesis in primary cultured AD-MSCs (n=3) after differentiation was stimulated for 8 days or in stable LMNA-KD cells generated via CRISPR-Cas9 (n=3). (C) Western blot analysis of the expression of LMNA under different conditions. LMNA was stably deleted from 7701 cells, as validated by western blotting. (D) CCK-8 assays showed inhibition in LMNA-KD AD-MSCs or LMNA-KO 7701 cell growth compared with WT cell growth (n=6). (E) TG and lactate synthesis were quantified in 7701 cells. Data are shown as the mean ± SD. ** $p < 0.01$, *** $p < 0.001$.

 doi:10.20944/preprints202207.0253.v1

3.3. LMNA and phosphorylation-activated AMPKα directly interacted in 7701 cells

In classical metabolic pathways, acetyl coenzyme A (acetyl-CoA) regulates metabolic flux. Excess acetyl-CoA from a high-glucose diet is used for *de novo* lipid synthesis and cholesterol synthesis [33] under normal conditions. The mitochondrial pyruvate carrier (MPC) 1/2 heterodimer in the inner mitochondrial membrane contributes to controlling the acetyl-CoA concentration in the cytosol by transporting pyruvate (a product of anaerobic glycolysis) into mitochondria [34]. Additionally, AMPKα, an energy sensor, coordinates the metabolism of glucose and lipids via its activation of Phosphofructokinase 2 (PFK2) in glycolysis and the phosphorylation of its substrate ACC1 in lipogenesis [35, 36]. In this context, after cell growth was synchronized by overnight starvation, we observed elevated pACC1-S79 and pAMPKα-T172 levels, decreased MPC1/2 and pAMPKα-S485 and FASN levels and no change in HMG-CoA reductase (HMGCR) levels in LMNA-knockout (KO) 7701 cells compared to wild-type (WT) 7701 cells (Figure 3A and B). We did not find a decrease in the mRNA level of ACC1 or MPC1/2 (Figure 3C). Furthermore, we performed immunoprecipitation experiments with endogenous proteins to determine whether pLMNA interacts with FASN, pACC1 or pAMPKα and whether LMNA interacts with pAMPKα (Figure 3D and 3E). The results supported the direct interaction between LMNA and pAMPKα-T172 (Figure 3E, highlighted in the red arrow). Through exogenous immunoprecipitation experiments with a Flag tag, we also validated that this direct interaction occurs at the N-terminal kinase domain of AMPKα (Figure 3F). These results strongly suggest that AMPK might be an important target by which LMNA mediates metabolism in liver tissue.

Preprints (www.preprints.org) | NOT PEER-REVIEWED | Posted: 18 July 2022 doi:10.20944/preprints202207.0253.v1

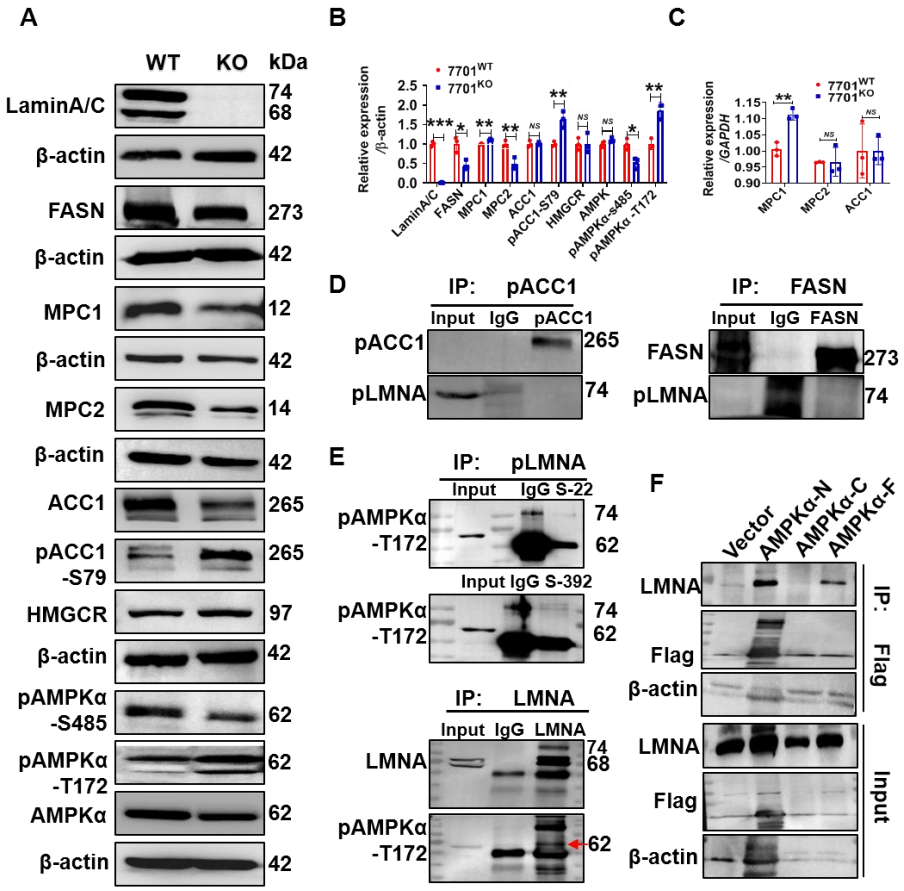

Figure 3. LMNA might be involved in *de novo* fatty acid synthesis through AMPK phosphorylation. (A) The expression levels of key enzymes and proteins involved in *de novo* fatty acid synthesis in *LMNA*-KO 7701 cells are shown with the corresponding quantitative plot (n=5) (B). (C) qRT-PCR was utilized to examine the mRNA expression of ACC1 and MPC1/2 in *LMNA*-KO 7701 cells (n=3). (D), (E) Co-IP assays were used to assess the endogenous interaction between pLMNA and FASN, pLMNA and pACC1, pLMNA and pAMPK or LMNA and pAMPK in *LMNA*-KO 7701 cells. IgG antibody was used as a negative control, and the input was used to examine the expression of FASN, pACC1, pLMNA and LMNA. (F) 7701 cells were transiently co-transfected with the plasmid containing LMNA cDNA and the AMPK-FLAG plasmid or control vector. Anti-FLAG antibody was used for pulldown of the cell lysates. Data are shown as the mean ± SD. * $p < 0.05$, ** $p < 0.01$.

3.4. AMPKα activation is closely associated with abnormal LMNA expression

To understand how LMNA-deletion activates AMPKα, lonafarnib was used to inhibit the farnesylation of LMNA. Disruption of LMNA maturation caused the activation of AMPK through its phosphorylation, and activated AMPK (phosphorylated AMPK), which in turn, targeted ACC, leading to intracellular changes in metabolic homeostasis in three liver cell lines (Figure 4A and D). Furthermore, we wanted to determine which form of LMNA is negatively associated with AMPKα activation. Therefore, we constructed different plasmids containing LMNA with mutations associated with FPLD, transfected them into 7701 cells and assessed changes in metabolic functions and key proteins in the 7701 cells. The schematic diagram in Figure 4C indicates the location of the mutation in the gene and protein structures. Via western blotting, we found that the mutant plasmids differentially affected the expression of mature LMNA (Figure 4B). Mutation 1 (M1, D230N) in the rod domain and mutation 2 (M2, G465D) in the lamin tail domain (LTD) could not rescue mature LMNA expression; however, both mutation 3 (M3, R482W) and mutation 4 (M4, T528R) could rescue. Furthermore, LMNA cDNA (SC1, 646 aa) successfully rescued mature LMNA expression, but full-length LMNA

Preprints (www.preprints.org) | NOT PEER-REVIEWED | Posted: 18 July 2022 doi:10.20944/preprints202207.0253.v1

cDNA (SC2, 661 aa, pre-LMNA) did not. Additionally, the increase in pAMPKα-T172 levels in the groups expressing LMNA cDNA, M3 or M4 was abrogated (Figure 4B). These findings show that pre-LMNA or mutations in the LMNA rod domain are closely related to pAMPKα-T172 levels. Furthermore, we examined the functional impact of these changes by measuring TG and lactic acid synthesis. The restored expression of LMNA through LMNA cDNA transfection successfully abrogated the increase in lactate synthesis and decrease in TG synthesis caused by LMNA deletion, but M3 and M4 in the LTD promoted lactate synthesis. Notably, phosphorylation inactivation due to M4 increased TG synthesis (Figure 4D), suggesting that modification of the LMNA tail is closely related to abnormal lipid metabolism and that phosphorylation at T528 plays a role in inhibiting lipid synthesis.

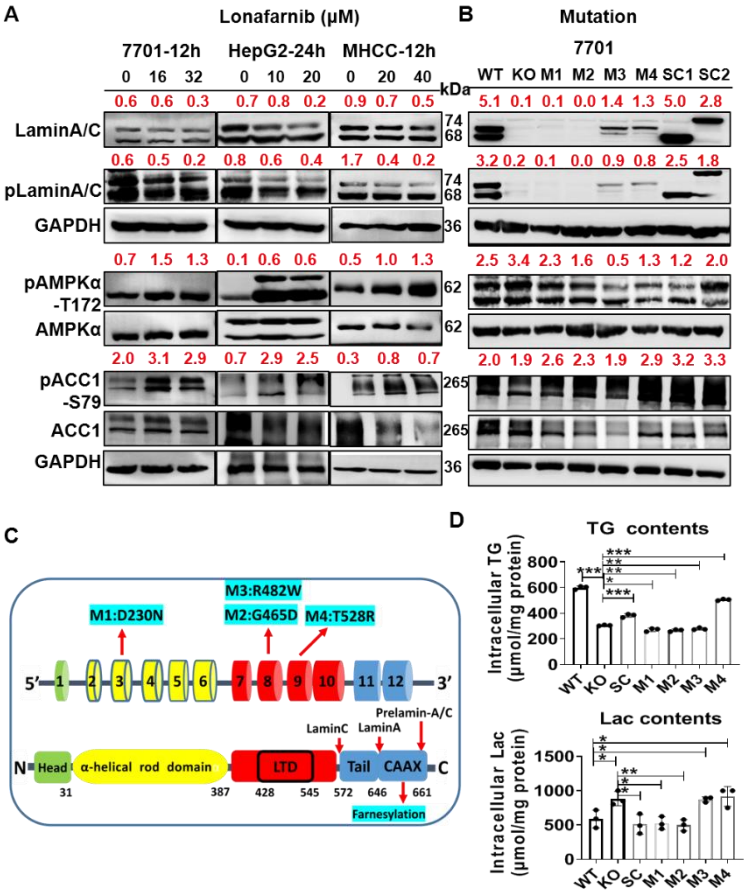

Figure 4. LMNA instability triggers AMPK activation. (A) Western blotting was used to assess concentration-dependent changes in LMNA, pLMNA, AMPK, pAMPK, pACC1 and ACC1 levels in 7701, HepG2 and MHCC cells treated with lonafarnib. The corresponding quantitative data were obtained by standardization with β-actin. (B) Western blotting was used to detect changes in LMNA, pLMNA, AMPK, pAMPK and FASN upon the rescue of LMNA expression via LMNA cDNA and LMNA mutants, and the corresponding semiquantitative data obtained via the β-actin correction are shown. SC1 is an abbreviation for the mature LMNA cDNA sequence, and SC2 is an abbreviation for the pre-LMNA sequence. (C) Mutations in the LMNA structure and sequence are shown: D203N in the rod domain and R482W, G465D, and T528R in the LTD. (D) TG and lactate synthesis was quantified in the different transfected groups. Data are shown as the mean of at least three independent experiments ± SD. ** $p < 0.01$, *** $p < 0.001$.

3.5. LMNA is not a substrate of AMPKα

Why was AMPKα activated in the presence of aberrant LMNA? Can pAMPKα-T172 in turn phosphorylate LMNA? After three cell lines were treated with a selective AMPK activator (A-769662) or an AMPK inhibitor (compound C), we found that both the inhibition and activation of AMPKα resulted in the downregulation of LMNA and pLMNA-

Preprints (www.preprints.org) | NOT PEER-REVIEWED | Posted: 18 July 2022 doi:10.20944/preprints202207.0253.v1

S22 (Figure 5A). Recent reports have revealed that A-769662 inhibits adipocyte differentiation, proteasomal activity, cell growth and DNA replication via an AMPK-independent mechanism [37-39]. As an important molecule for differentiation, LMNA is presumably a direct target of A-769662.

In cell models treated with high glucose (25 mM), we found that the level of pAMPKα-T172 was reduced and that LMNA phosphorylation was increased (Figure 5B and D), suggesting that the phosphorylation of LMNA is independent of AMPK activation. Together, our data indicate that decreased AMPK activity promotes lipid synthesis (Figure 5C) in condition of high glucose. Furtherly, we adopted endogenous IP of LMNA in the nucleus and identified interacting enzymes with LMNA that are closely related to ATP synthesis through mass spectrometry analysis, such as transitional endoplasmic reticulum ATPase and ADP/ATP translocase 2 (Table 1 and Figure S2). LMNA may be involved in regulating ATP metabolism in the nucleus. Additionally, pLMNA and FASN expression were increased under high-glucose conditions (25 mM), consistent with our findings in obese model animals (Figure 5B and Figure 1A). This suggests that pLMNA is an indicator of increased lipid metabolism and synthesis.

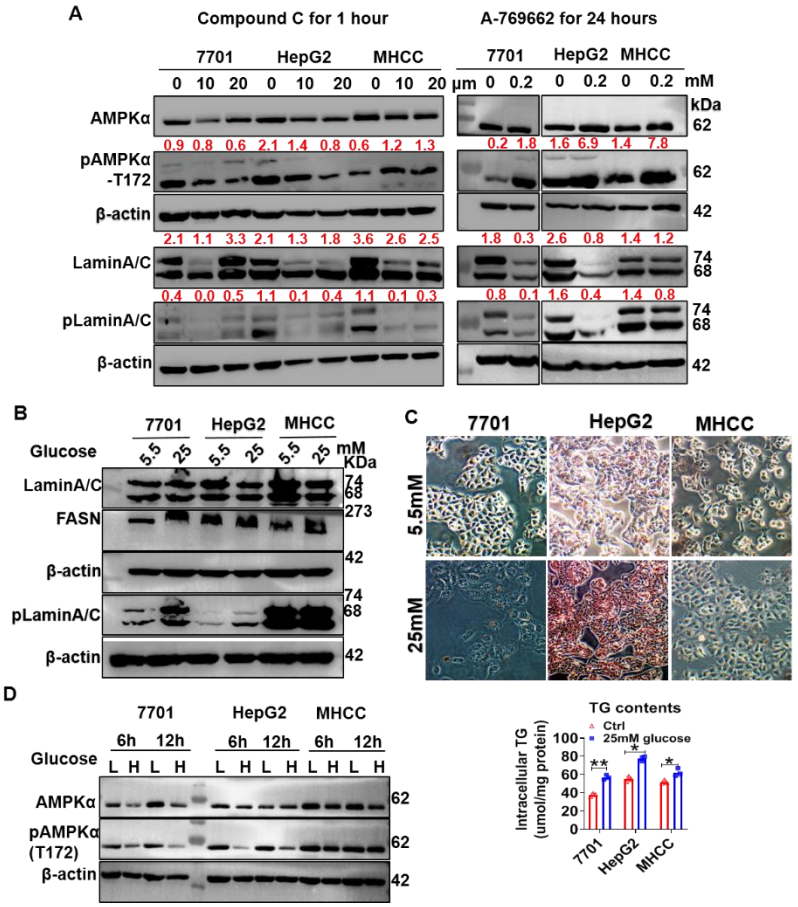

Figure 5. AMPK activation and inhibition were not accompanied by changes in pLMNA. (A) Left: AMPK activation was inhibited by compound C in a concentration-dependent manner. Right: When AMPK was activated with A769662, LMNA and pLMNA were still downregulated in 7701, HepG2 and MHCC cells. Semiquantitative values from blots are displayed. (B) and (D) Treatment with 25 mM glucose promoted LMNA phosphorylation and inhibited AMPK activation. (C) Oil red O staining was carried out to show TG synthesis. TG synthesis was quantified. * $p < 0.05$, ** $p < 0.01$, *** $p < 0.001$. L=5.5mM, H=25mM glucose.

Preprints (www.preprints.org) | NOT PEER-REVIEWED | Posted: 18 July 2022 doi:10.20944/preprints202207.0253.v1

Table 1. Mass spectrometry detected partners of intranuclear LMNA

Peptides	PSMs[1]	Group Description
32	279	Prelamin-A/C OS=Homo sapiens OX=9606 GN=LMNA
10	61	Lamin-B1 OS=Homo sapiens OX=9606 GN=LMNB1
19	36	Keratin, type II cytoskeletal 1 OS=Homo sapiens OX=9606 GN=KRT1
12	20	Keratin, type II cytoskeletal 2 epidermal OS=Homo sapiens OX=9606 GN=KRT2
7	20	Tubulin alpha-1B chain OS=Homo sapiens OX=9606 GN=TUBA1B
9	19	Keratin, type I cytoskeletal 9 OS=Homo sapiens OX=9606 GN=KRT9
6	16	Tubulin alpha-1C chain OS=Homo sapiens OX=9606 GN=TUBA1C
4	16	Lamin-B2 OS=Homo sapiens OX=9606 GN=LMNB2
8	13	Heat shock protein HSP 90-beta OS=Homo sapiens OX=9606 GN=HSP90AB1
6	13	Tubulin beta chain OS=Homo sapiens OX=9606 GN=TUBB
7	12	Heat shock 70 kDa protein 1B OS=Homo sapiens OX=9606 GN=HSPA1B
7	12	Actin, cytoplasmic 1 OS=Homo sapiens OX=9606 GN=ACTB
8	11	Keratin, type I cytoskeletal 10 OS=Homo sapiens OX=9606 GN=KRT10
7	11	Keratin, type II cytoskeletal 6B OS=Homo sapiens OX=9606 GN=KRT6B
5	10	Elongation factor 1-alpha 1 OS=Homo sapiens OX=9606 GN=EEF1A1
1	10	Serum albumin OS=Homo sapiens OX=9606 GN=ALB
8	9	Keratin, type II cytoskeletal 5 OS=Homo sapiens OX=9606 GN=KRT5
7	8	Keratin, type II cytoskeletal 6C OS=Homo sapiens OX=9606 GN=KRT6C
4	8	Heterogeneous nuclear ribonucleoprotein H OS=Homo sapiens OX=9606 GN=HNRNPH1
6	7	Nucleolar RNA helicase 2 OS=Homo sapiens OX=9606 GN=DDX21
7	7	Keratin, type I cytoskeletal 16 OS=Homo sapiens OX=9606 GN=KRT16
4	7	Alpha-enolase OS=Homo sapiens OX=9606 GN=ENO1
4	7	Heat shock cognate 71 kDa protein OS=Homo sapiens OX=9606 GN=HSPA8
5	6	Pyruvate kinase PKM OS=Homo sapiens OX=9606 GN=PKM
4	6	Elongation factor 2 OS=Homo sapiens OX=9606 GN=EEF2
5	5	T-complex protein 1 subunit alpha OS=Homo sapiens OX=9606 GN=TCP1
3	3	Transitional endoplasmic reticulum ATPase OS=Homo sapiens OX=9606 GN=VCP
2	2	ADP/ATP translocase 2 OS=Homo sapiens OX=9606 GN=SLC25A5
1	1	Fatty acid-binding protein 5 OS=Homo sapiens OX=9606 GN=FABP5
1	1	Proliferation-associated protein 2G4 OS=Homo sapiens OX=9606 GN=PA2G4

[1] PSMs is the abbreviation of the peptide-spectrum matches.

3.6. Combined targeting of AMPKα and LMNA effectively inhibited HCC cell growth

Liver cancer is strongly associated with abnormal lipid metabolism. Do metabolic syndrome and liver cancer share a common mechanism? According to analysis with the TCGA database, LMNA expression gradually increased with liver cancer grade, in line with the findings of HCC cell lines with different degrees of malignancy (Figure 6A and B). HCC patients with higher LMNA levels exhibited shorter survival than those with low/medium LMNA levels (Figure 6A, right). Both HepG2 and MHCC cells could not survive more than three days under LMNA-KD conditions. These findings indicate that LMNA acts as an oncogene in HCC. We also found that pAMPK-T172 levels increased

Preprints (www.preprints.org) | NOT PEER-REVIEWED | Posted: 18 July 2022 doi:10.20944/preprints202207.0253.v1

in a concentration-dependent manner when HepG2 or MHCC cells were treated with lonafarnib (Figure 6C). In addition, lonafarnib reduced the expression of HMGCR (β-hydroxy-β-methylglutaryl coenzyme A reductase), the rate-limiting enzyme in cholesterol synthesis, in a concentration-dependent manner. However, because pAMPK-T172 can promote glycolysis to maintain energy in cancer cells, the synergistic use of lonafarnib and glucose-lowering therapies should more efficiently inhibit the growth of HCC cells. As expected, 4 μM lonafarnib combined with metformin significantly inhibited the growth of HepG2 and MHCC cells compared with their growth upon treatment with lonafarnib alone (Figure 6D).

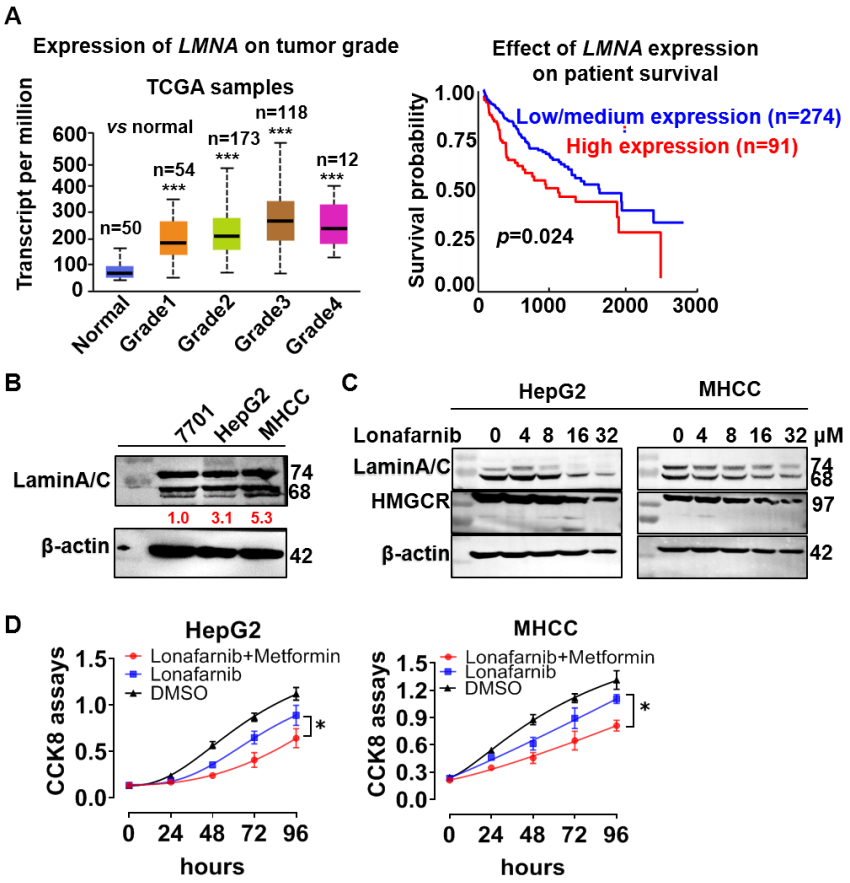

Figure 6. Lonafarnib combined with metformin significantly inhibited the growth of HepG2 and MHCC cells. (A) Left: LMNA expression gradually increased with liver cancer grade based on data from the TCGA database (n=407). Right: The survival of patients with high LMNA levels was significantly shorter than that of patients with low/medium LMNA levels. (B) LMNA levels in HCC cell lines show different degrees of malignancy and the corresponding statistical data (n=3). (C) Western blotting showed that lonafarnib reduced the expression of LMNA and HMGCR in a concentration-dependent manner. (D) CCK-8 assays were carried out to assess the growth of cancer cells treated with lonafarnib and metformin. Three independent experiments were performed. Data are shown as the mean ± SD. * $p < 0.05$, ** $p < 0.01$.

4. Discussion

LMNA is known to play a role in promoting differentiation, especially in mesenchymal stem cells and even in cancer cells [40, 41]. Consistent with this function, our experiments confirmed that LMNA KD in AD-MSCs of rats hindered adipocyte development and proliferation and then reduced lipid synthesis. However, pLMNA is used as an indicator of mitosis and cell proliferation [42, 43]. Since the depolymerization of LMNA via phosphorylation during mitosis allows pLMNA to enter the cytoplasm, the functions of LMNA and pLMNA should differ. Immunohistochemical staining of human liver and fat tissues revealed that LMNA localized to the nuclear membrane and that pLMNA was

 doi:10.20944/preprints202207.0253.v1

distributed mainly in the cytoplasm and around lipid droplets. Using the 7701-cell line as our model, we identified additional functions of LMNA linked to energy metabolism and additional functions of pLMNA linked to *de novo* lipid synthesis that has not yet been reported in the literature.

Lipodystrophies are characterized by the loss of adipose tissue [44]. LMNA-linked FPLD leads to partial ectopic lipodystrophy and metabolic complications including hyperglycemia, hypertriglyceridemia and fatty liver [45]. However, we wondered whether LMNA can coordinate metabolic pathways in the liver, the central metabolic organ. Furthermore, is this coordination partially responsible for some acquired metabolic syndromes? First, we induced a rat model of obesity by high-fat diet feeding and explored whether LMNA participates in TG metabolism. Two key enzymes in lipid synthesis, ACC1 and FASN, were found to be altered at the protein level in the animal liver tissues, and the change in FASN levels was positively correlated with the change in pLMNA-S392 or pLMNA-S22 levels. The expression of both pLMNA-S22/392 and FASN increased in a time-dependent manner in 7701 and HepG2 cells stimulated with high glucose. Additionally, the NetPhos 3.1 server predicted that pLMNA-S392 has kinase activity. Therefore, we speculate the existence of a direct regulatory relationship between LMNA and AMPK via phosphorylation and that this regulatory relationship can partly explain the mechanism of hyperglyceridemia in FPLD and hepatocarcinogenesis. However, disappointingly, no interaction between pLMNA-S392 and FASN or pLMNA-S392 and pACC1-S79 was found in 7701 cells. In the glucose-induced cell models, increased pLMNA levels were not accompanied by the upregulation of pAMPKα. In contrast, two AMPKα activators, A769662 and AICAR (Figure S1) downregulated LMNA and pLMNA levels, indicating that LMNA is also not a substrate of pAMPKα.

To further investigate the related mechanism, we constructed a stable LMNA-KO 7701 cell line and found pAMPKα-T172 levels to be increased, accompanied by a decrease in TG synthesis and an increase in lactate. AMPK, which belongs to the Ser/Thr protein kinase family, contains three catalytic subunits, α, β and γ. AMPKα is a known inhibitor of lipid synthesis via its direct serine phosphorylation of ACC1-79, which promotes glycolysis and fatty acid oxidation, but high glucose levels can inhibit AMPK activation [46]. Importantly, our experiment showed that LMNA pulled down the pAMPKα-T172 protein in 7701 cells; however, pLMNA-S392 did not. Based on the Human Protein Atlas, AMPKα in single human cells mainly localizes to nuclear speckles [47]. In addition, it also localizes to the cytosol. The laminA protein is the principal protein in nuclear speckles [48, 49]. Since no interaction between pLMNA-S392 and pAMPKα-T172 was identified, AMPK activation should correlate with the structural stability of the nucleus. By endogenous mass spectrometry in 293T cells, we identified that the main proteins recruited by LMNA are functionally enriched in keratinocyte migration, protein refolding, intermediate filament cytoskeleton organization, NADH metabolic process, and positive regulation of ATP biosynthetic process etc., suggesting that LMNA has the function of regulating ATP metabolism. The ClinVar database contains a summary of many FPLD-associated LMNA mutations; among them, D230N in the α-helical rod domain and R482W, G465D, and T528R in the LTD were selected and mutated in our model. Coincidentally, the T528R mutation prevents phosphorylation and has no kinase activity, as predicted with the NetPhos 3.1 server. When these mutant plasmids and control normal plasmids were transfected into the 7701-KO cell line, the increase in pAMPKα-T172 in the KO group was alleviated upon LMNA re-expression. The plasmid containing mature LMNA cDNA successfully abrogated the increase in pAMPKα-T172 in the KO group; however, pre-LMNA cDNA did not. We determined that the processing of pre-LMNA with an altered structure was difficult when the cDNA sequence was expressed *in vitro*. Mutations at codons 230 and 465 of LMNA resulted in the loss of LMNA protein expression and decreased TG synthesis, like the effects of LMNA KO. Due to rescued expression of laminA upon its mutation at codons 482 and 528, the increase in pAMPKα-T172 was alleviated. The T528R mutation caused an increase in the synthesis of both lactate and lipids in 7701 cells; however, R482W increased the synthesis of only lactate. These data suggest that LMNA regulates AMPK

 doi:10.20944/preprints202207.0253.v1

activation through its structural stability. Under normal conditions, LMNA inhibited AMPK phosphorylation and activation to regulate overall metabolism in 7701 cells. Mutation-induced disruption in the structural stability of the nucleus can interfere with glycolipid metabolic homeostasis. To further validate this hypothesis, upon inhibiting LMNA maturation and the consequent destabilization of the nuclear structure using farnesylation inhibitors, we also detected increased pAMPKα-T172 levels in 7701, HepG2 and MHCC cells.

In addition, we found in 7701, HepG2 and MHCC cells that pLMNA-S392/22 plays a role in lipid synthesis. However, LMNA proteins phosphorylated at different sites have different effects on lipid metabolism. The data suggest that pLMNA-T528 inhibited lipid synthesis in 7701 cells, while pLMNAS-392/22 promoted lipid synthesis. pLMNA is mainly involved in envelope disintegration during mitosis. Thus, LMNA and AMPKα phosphorylation should be two independent events regulated by LMNA in different stages of the cell cycle. Numerous studies have found a link between aberrant lipid metabolism and liver cancer. LMNA overexpression is associated with the malignancy of liver cancer and patient survival. In our study, we found that the dysregulation of pLMNA is likely a common mechanism of abnormal lipid metabolism and liver cancer. AMPKα activation is an important pathway in LMNA-mediated glycolipid metabolism. The combination of glucose restriction and targeting LMNA would undoubtedly increase the efficiency of HCC treatments. This requires further validation in clinical trials.

5. Conclusions

In summary, LMNA KO inhibited *de novo* fatty acid synthesis via AMPK phosphorylation, which elevated the level of pACC1-S79 and might also have downregulated MPC1/2 to increase the cytosolic pyruvate concentration and stimulate lactic acid production. During mitosis, pLMNA promotes *de novo* fatty acid synthesis to maintain the membrane structure.

Supplementary Materials: The following supporting information can be downloaded at: www.mdpi.com/xxx/s1, Figure S1: LMNA and pLMNA from 3 cell lines were downregulated by AICAR in a concentration-dependent manner; Figure S2: Mass spectrometry analysis of intranuclear immunoprecipitants interacting with LMNA; Table S1: Primers in experiments.

Author Contributions: "Conceptualization, Lu Kong.; validation, Rong-hui Yang.; formal analysis, Ying Zhou., Jia-jie Yang., and Yuan yuan.; investigation, Ying Zhou., Jia-jie Yang., Yuan Cheng., and Ge-xuan Feng; data curation, Ying Zhou.,Jia-jie Yang.,Li-yong Wang.; writing—original draft preparation, Lu Kong.; writing—review and editing, Lu kong.; visualization, Yuan Cheng.,Ge-xuan Feng., Rong-hui Yang.,Yuan Yuan; supervision, Lu kong.; project administration, Lu kong; funding acquisition, Lu kong. All authors have read and agreed to the published version of the manuscript."

Funding: This research was funded by the National Nature Science Foundation of China., grant number 81672834 and 81272406.

Institutional Review Board Statement: Human normal liver tissue and adipose tissue microarrays are commercially purchased and approved by the ethics committee of Capital Medical University (2018/01/12). Animal experiments were also reviewed and approved by the Animal Ethics Committee of Capital Medical University (AEEI-2019-093). The study was conducted in accordance with the Declaration of Helsinki.

Data Availability Statement: All data generated or analyzed during this study and its supplementary information files are included in this published article. Cell lines and most reagents generated for this study are available upon request.

Acknowledgments: We acknowledged Dr Yang Chuan-Zhen and Dr Shan Lin for technical support..

Conflicts of Interest: The authors declare no conflict of interest.

Abbreviations

H&E, Haematoxylin-eosin;

 doi:10.20944/preprints202207.0253.v1

FPLD, familial partial lipodystrophy of Dunnigan;
AD-MSCs, adipose-derived mesenchymal stem cells;
pLMNA, phosphorylated LMNA;
ACC1, acetyl-CoA-carboxylase 1;
FASN, fatty acid synthase;
PC, prostate cancer;
HCC, hepatocellular carcinoma;
CRC, metastatic colorectal cancer;
HGPS, Hutchinson-Gilford syndrome;
FTIs, Farnesyltransferase inhibitors;
AMPK, Adenosine 5'-monophosphate activated protein kinase;
TG, triglyceride;
Acetyl-CoA, acetyl coenzyme A;
MPC, Mitochondrial Pyruvate Carrier;
WT, wild type

References

1. Saez A, Herrero-Fernandez B, Gomez-Bris R, Somovilla-Crespo B, Rius C, Gonzalez-Granado JM. Lamin A/C and the Immune System: One Intermediate Filament, Many Faces. *Int J Mol Sci* 2020; 21: 6109.
2. Fiserova J, Goldberg MW. Relationships at the nuclear envelope: lamins and nuclear pore complexes in animals and plants. *Biochem Soc Trans* 2010; 38: 829-831.
3. Shilo A, Tosto FA, Rausch JW, Le Grice SFJ, Misteli T. Interplay of primary sequence, position and secondary RNA structure determines alternative splicing of LMNA in a pre-mature aging syndrome. *Nucleic Acids Res* 2019; 47: 5922-5935.
4. Capitanchik C, Dixon CR, Swanson SK, Florens L, Kerr ARW, Schirmer EC. Analysis of RNA-Seq datasets reveals enrichment of tissue-specific splice variants for nuclear envelope proteins. *Nucleus* 2018; 9: 410-430.
5. Sinensky M, Fantle K, Trujillo M, McLain T, Kupfer A, Dalton M. The processing pathway of prelamin A. *J Cell Sci* 1994; 107 (Pt 1): 61-67.
6. Perrin S, Cremer J, Faucher O, Reynes J, Dellamonica P, Micallef J et al. HIV protease inhibitors do not cause the accumulation of prelamin A in PBMCs from patients receiving first line therapy: the ANRS EP45 "aging" study. *PLoS One* 2012; 7: e53035.
7. Reddy S, Comai L. Lamin A, farnesylation and aging. *Exp Cell Res* 2012; 318: 1-7.
8. Makarov AA, Zou J, Houston DR, Spanos C, Solovyova AS, Cardenal-Peralta C et al. Lamin A molecular compression and sliding as mechanisms behind nucleoskeleton elasticity. *Nat Commun* 2019; 10: 3056.
9. Burke B, Stewart CL. The nuclear lamins: flexibility in function. *Nat Rev Mol Cell Biol* 2013; 14: 13-24.
10. Wang AS, Kozlov SV, Stewart CL, Horn HF. Tissue specific loss of A-type lamins in the gastrointestinal epithelium can enhance polyp size. *Differentiation* 2015; 89: 11-21.
11. Zuo L, Zhao H, Yang R, Wang L, Ma H, Xu X et al. Lamin A/C might be involved in the EMT signalling pathway. *Gene* 2018; 663: 51-64.
12. Liu H, Li D, Zhou L, Kan S, He G, Zhou K et al. LMNA functions as an oncogene in hepatocellular carcinoma by regulating the proliferation and migration ability. *J Cell Mol Med* 2020; 24: 12008-12019.
13. Lin YT, Chien KY, Wu CC, Chang WY, Chu LJ, Chen MC et al. Super-SILAC mix coupled with SIM/AIMS assays for targeted verification of phosphopeptides discovered in a large-scale phosphoproteome analysis of hepatocellular carcinoma. *J Proteomics* 2017; 157: 40-51.
14. Sartore-Bianchi A, Ardini E, Bosotti R, Amatu A, Valtorta E, Somaschini A et al. Sensitivity to Entrectinib Associated With a Novel LMNA-NTRK1 Gene Fusion in Metastatic Colorectal Cancer. *J Natl Cancer Inst* 2016; 108: djv306.
15. Russo M, Misale S, Wei G, Siravegna G, Crisafulli G, Lazzari L et al. Acquired Resistance to the TRK Inhibitor Entrectinib in Colorectal Cancer. *Cancer Discov* 2016; 6: 36-44.
16. Kilanczyk E, Graczyk A, Ostrowska H, Kasacka I, Lesniak W, Filipek A. S100A6 is transcriptionally regulated by beta-catenin and interacts with a novel target, lamin A/C, in colorectal cancer cells. *Cell Calcium* 2012; 51: 470-477.
17. Neilan EG. Laminopathies, other progeroid disorders, and aging: common pathogenic themes and possible treatments. *Am J Med Genet A* 2009; 149A: 563-566.
18. Decaudain A, Vantyghem MC, Guerci B, Hecart AC, Auclair M, Reznik Y et al. New metabolic phenotypes in laminopathies: LMNA mutations in patients with severe metabolic syndrome. *J Clin Endocrinol Metab* 2007; 92: 4835-4844.
19. Haithcock E, Dayani Y, Neufeld E, Zahand AJ, Feinstein N, Mattout A et al. Age-related changes of nuclear architecture in Caenorhabditis elegans. *Proc Natl Acad Sci U S A* 2005; 102: 16690-16695.
20. Gonzalo S, Kreienkamp R, Askjaer P. Hutchinson-Gilford Progeria Syndrome: A premature aging disease caused by LMNA gene mutations. *Ageing Res Rev* 2017; 33: 18-29.
21. Piekarowicz K, Machowska M, Dzianisava V, Rzepecki R. Hutchinson-Gilford Progeria Syndrome-Current Status and Prospects for Gene Therapy Treatment. *Cells* 2019; 8:88.

22. Oldenburg AR, Delbarre E, Thiede B, Vigouroux C, Collas P. Deregulation of Fragile X-related protein 1 by the lipodystrophic lamin A p.R482W mutation elicits a myogenic gene expression program in preadipocytes. *Hum Mol Genet* 2014; 23: 1151-1162.
23. Bertrand AT, Renou L, Papadopoulos A, Beuvin M, Lacene E, Massart C et al. DelK32-lamin A/C has abnormal location and induces incomplete tissue maturation and severe metabolic defects leading to premature death. *Hum Mol Genet* 2012; 21: 1037-1048.
24. Youssef SJ, Macielak RJ, Schimmenti LA, Chatzopoulos K, Price DL. Hypopharyngeal Squamous Cell Carcinoma in Sisters with LMNA Associated Familial Partial Lipodystrophy: A Case Report and Review of the Literature. *Ann Otol Rhinol Laryngol* 2020; 129: 1243-1246.
25. Melvin A, Stears A, Savage DB. Recent developments in lipodystrophy. *Curr Opin Lipidol* 2019; 30: 284-290.
26. Vasandani C, Li X, Sekizkardes H, Adams-Huet B, Brown RJ, Garg A. Diagnostic Value of Anthropometric Measurements for Familial Partial Lipodystrophy, Dunnigan Variety. *J Clin Endocrinol Metab* 2020; 105:2132-2141.
27. Miranda M, Chacon MR, Gutierrez C, Vilarrasa N, Gomez JM, Caubet E et al. LMNA mRNA expression is altered in human obesity and type 2 diabetes. *Obesity* (Silver Spring) 2008; 16: 1742-1748.
28. Wegner L, Andersen G, Sparso T, Grarup N, Glumer C, Borch-Johnsen K et al. Common variation in LMNA increases susceptibility to type 2 diabetes and associates with elevated fasting glycemia and estimates of body fat and height in the general population: studies of 7,495 Danish whites. *Diabetes* 2007; 56: 694-698.
29. Finley J. Alteration of splice site selection in the LMNA gene and inhibition of progerin production via AMPK activation. *Med Hypotheses* 2014; 83: 580-587.
30. Dhillon S. Lonafarnib: First Approval. *Drugs* 2021; 81: 283-289.
31. Wong NS, Morse MA. Lonafarnib for cancer and progeria. *Expert Opin Investig Drugs* 2012; 21: 1043-1055.
32. Araujo-Vilar D, Lattanzi G, Gonzalez-Mendez B, Costa-Freitas AT, Prieto D, Columbaro M et al. Site-dependent differences in both prelamin A and adipogenic genes in subcutaneous adipose tissue of patients with type 2 familial partial lipodystrophy. *J Med Genet* 2009; 46: 40-48.
33. Mahmood S, Birkaya B, Rideout TC, Patel MS. Lack of mitochondria-generated acetyl-CoA by pyruvate dehydrogenase complex downregulates gene expression in the hepatic de novo lipogenic pathway. *Am J Physiol Endocrinol Metab* 2016; 311: E117-127.
34. Vanderperre B, Herzig S, Krznar P, Horl M, Ammar Z, Montessuit S et al. Embryonic Lethality of Mitochondrial Pyruvate Carrier 1 Deficient Mouse Can Be Rescued by a Ketogenic Diet. *PLoS Genet* 2016; 12: e1006056.
35. Yu YH, Zhang P, Wang CL, Liu JG, Li P, Zhang DW. Panax quinquefolium saponin Optimizes Energy Homeostasis by Modulating AMPK-Activated Metabolic Pathways in Hypoxia-Reperfusion Induced Cardiomyocytes. *Chin J Integr Med* 2020; 27:613-620.
36. Ben Djoudi Ouadda A, Levy E, Ziv E, Lalonde G, Sane AT, Delvin E et al. Increased hepatic lipogenesis in insulin resistance and Type 2 diabetes is associated with AMPK signalling pathway up-regulation in Psammomys obesus. *Biosci Rep* 2009; 29: 283-292.
37. Pizzo E, Varcamonti M, Di Maro A, Zanfardino A, Giancola C, D'Alessio G. Ribonucleases with angiogenic and bactericidal activities from the Atlantic salmon. *FEBS J* 2008; 275: 1283-1295.
38. Zhou Y, Wang D, Zhu Q, Gao X, Yang S, Xu A et al. Inhibitory effects of A-769662, a novel activator of AMP-activated protein kinase, on 3T3-L1 adipogenesis. *Biol Pharm Bull* 2009; 32: 993-998.
39. Peyton KJ, Liu XM, Yu Y, Yates B, Durante W. Activation of AMP-activated protein kinase inhibits the proliferation of human endothelial cells. *J Pharmacol Exp Ther* 2012; 342: 827-834.
40. Ocampo A, Reddy P, Martinez-Redondo P, Platero-Luengo A, Hatanaka F, Hishida T et al. In Vivo Amelioration of Age-Associated Hallmarks by Partial Reprogramming. *Cell* 2016; 167: 1719-1733 e1712.
41. Nardella M, Guglielmi L, Musa C, Iannetti I, Maresca G, Amendola D et al. Down-regulation of the Lamin A/C in neuroblastoma triggers the expansion of tumor initiating cells. *Oncotarget* 2015; 6: 32821-32840.
42. Liu SY, Ikegami K. Nuclear lamin phosphorylation: an emerging role in gene regulation and pathogenesis of laminopathies. *Nucleus* 2020; 11: 299-314.
43. Torvaldson E, Kochin V, Eriksson JE. Phosphorylation of lamins determine their structural properties and signaling functions. Nucleus 2015; 6: 166-171.
44. Garg A. Lipodystrophies. *Am J Med* 2000; 108: 143-152.
45. Knebel B, Muller-Wieland D, Kotzka J. Lipodystrophies-Disorders of the Fatty Tissue. Int J Mol Sci 2020; 21:8778.
46. Jiang P, Ren L, Zhi L, Yu Z, Lv F, Xu F et al. Negative regulation of AMPK signaling by high glucose via E3 ubiquitin ligase MG53. *Mol Cell* 2021; 81: 629-637 e625.
47. Kazgan N, Williams T, Forsberg LJ, Brenman JE. Identification of a nuclear export signal in the catalytic subunit of AMP-activated protein kinase. *Mol Biol Cell* 2010; 21: 3433-3442.
48. Barutcu AR, Wu M, Braunschweig U, Dyakov BJA, Luo Z, Turner KM et al. Systematic mapping of nuclear domain-associated transcripts reveals speckles and lamina as hubs of functionally distinct retained introns. Mol Cell 2022; 82: 1035-1052 e1039.
49. Meng F, Na I, Kurgan L, Uversky VN. Compartmentalization and Functionality of Nuclear Disorder: Intrinsic Disorder and Protein-Protein Interactions in Intra-Nuclear Compartments. *Int J Mol Sci* 2015; 17:24.